Near-infrared grating-assisted SPR optical fiber sensors: design rules for ultimate refractometric sensitivity

Christophe Caucheteur,[1,*] Valérie Voisin,[1] and Jacques Albert,[2]

[1]*Electromagnetism and Telecommunication Department, Université de Mons, 31 Boulevard Dolez, Mons, 7000, Belgium*

[2]*Department of Electronics, Carleton University, 1125 Colonel By Drive, Ottawa, Ontario K1S 5B6, Canada*

[*]*christophe.caucheteur@umons.ac.be*

Abstract: Plasmonic optical fiber sensors are continuously developed for (bio)chemical sensing purposes. Recently, surface plasmon resonance (SPR) generation was achieved in gold-coated tilted fiber Bragg gratings (TFBGs). These sensors probe the surrounding medium with near-infrared narrowband resonances, which enhances both the penetration depth of the evanescent field in the external medium and the wavelength resolution of the interrogation. They constitute a unique configuration to probe all the fiber cladding modes individually. We use them to analyze the modal distribution of gold-coated telecommunication-grade optical fibers immersed in aqueous solutions. Theoretical investigations with a finite-difference complex mode solver are confirmed by experimental data obtained on TFBGs. We show that the refractometric sensitivity varies with the mode order and that the global SPR envelope shift in response to surrounding refractive index (SRI) changes higher than 1e-2 RIU (refractive index unit) can be ~25% bigger than the local SPR mode shift arising from SRI changes limited to 1e-4 RIU. We bring clear evidence that the optimum gold thickness for SPR generation lies in the range between 50 and 70 nm while a cladding diameter decrease from 125 µm to 80 µm enhances the refractometric sensitivity by ~20%. Finally, we demonstrate that the ultimate refractometric sensitivity of cladding modes is ~550 nm/RIU when they are probed by gold-coated TFBGs.

OCIS codes: (060.2370) Fiber optics sensors; (240.6680) Surface plasmons; (060.3735) Fiber Bragg gratings.

References and links

1. E. Kretschmann and H. Raether, "Radiative decay of non radiative surface plasmon excited by light," Z. Naturforsch. B **23**, 2135 (1968).
2. R. Jorgenson and S. Yee, "A fiber-optic chemical sensor based on surface plasmon resonance," Sens. Actuators B Chem. **12**(3), 213–220 (1993).
3. A. Trouillet, C. Ronot-Triol, C. Veillas, and H. Gagnaire, "Chemical sensing by surface plasmon resonance in a multimode optical fiber," Pure Appl. Opt. **5**(2), 227–237 (1997).
4. J. Homola, "Optical fiber sensor based on surface plasmon excitation," Sens. Actuators B Chem. **29**(1-3), 401–405 (1995).
5. M. H. Chiu, S. F. Wang, and R. S. Chang, "D-type fiber biosensor based on surface-plasmon resonance technology and heterodyne interferometry," Opt. Lett. **30**(3), 233–235 (2005).
6. Y. L. Lo, C. H. Chuang, and Z. W. Lin, "Ultra-high sensitivity polarimetric strain sensor based upon D-shaped optical fiber and surface plasmon resonance technology," Opt. Lett. **36**(13), 2489–2491 (2011).
7. R. K. Verma, A. K. Sharma, and B. D. Gupta, "Surface plasmon resonance based tapered fiber optic sensor with different taper profiles," Opt. Commun. **281**(6), 1486–1491 (2008).
8. V. V. R. Sai, T. Kundu, and S. Mukherji, "Novel U-bent fiber optic probe for localized surface plasmon resonance based biosensor," Biosens. Bioelectron. **24**(9), 2804–2809 (2009).

#230719 - $15.00 USD Received 16 Dec 2014; revised 15 Jan 2015; accepted 23 Jan 2015; published 30 Jan 2015

9. T. Schuster, R. Herschel, N. Neumann, and C. G. Schaffer, "Miniaturized long-period fiber grating assisted surface plasmon resonance sensor," J. Lightwave Technol. **30**(8), 1003–1008 (2012).
10. J. Albert, L.-Y. Shao, and C. Caucheteur, "Tilted fiber Bragg grating sensors," Laser Photonics Rev. **7**(1), 83–108 (2013).
11. Y. S. Dwivedi, A. K. Sharma, and B. D. Gupta, "Influence of design parameters on the performance of a surface plasmon sensor based fiber optic sensor," Plasmonics **3**(2-3), 79–86 (2008).
12. J. Pollet, F. Delport, K. P. F. Janssen, K. Jans, G. Maes, H. Pfeiffer, M. Wevers, and J. Lammertyn, "Fiber optic SPR biosensing of DNA hybridization and DNA-protein interactions," Biosens. Bioelectron. **25**(4), 864–869 (2009).
13. F. Baldini, M. Brenci, F. Chiavaioli, A. Giannetti, and C. Trono, "Optical fibre gratings as tools for chemical and biochemical sensing," Anal. Bioanal. Chem. **402**(1), 109–116 (2012).
14. C. Caucheteur, T. Guo, and J. Albert, "Review of plasmonic fiber optic biochemical sensors: improving the limit of detection," Anal. Bioanal. Chem. (2015), doi:10.1007/s00216-014-8411-6.
15. P. Offermans, M. C. Schaafsma, S. R. K. Rodriguez, Y. Zhang, M. Crego-Calama, S. H. Brongersma, and J. Gómez Rivas, "Universal scaling of the figure of merit of plasmonic sensors," ACS Nano **5**(6), 5151–5157 (2011).
16. Y. Y. Shevchenko, C. Chen, M. A. Dakka, and J. Albert, "Polarization-selective grating excitation of plasmons in cylindrical optical fibers," Opt. Lett. **35**(5), 637–639 (2010).
17. Y. Y. Shevchenko, T. J. Francis, D. A. Blair, R. Walsh, M. C. DeRosa, and J. Albert, "In situ biosensing with a surface Plasmon resonance fiber grating aptasensor," Anal. Chem. **83**(18), 7027–7034 (2011).
18. V. Voisin, J. Pilate, P. Damman, P. Mégret, and C. Caucheteur, "Highly sensitive detection of molecular interactions with plasmonic optical fiber grating sensors," Biosens. Bioelectron. **51**, 249–254 (2014).
19. J. Albert, S. Lepinay, C. Caucheteur, and M. C. Derosa, "High resolution grating-assisted surface plasmon resonance fiber optic aptasensor," Methods **63**(3), 239–254 (2013).
20. H. Raether, *Surface Plasmons on Smooth and Rough Surfaces and on Gratings*, (Springer, 1988).
21. H. Suzuki, M. Sugimoto, Y. Matsui, and J. Kondoh, "Effects of gold film thickness on spectrum profile and sensitivity of a multimode-optical-fiber SPR sensor," Sens. Actuators B Chem. **132**(1), 26–33 (2008).
22. C. Caucheteur, Y. Y. Shevchenko, L.-Y. Shao, M. Wuilpart, and J. Albert, "High resolution interrogation of tilted fiber grating SPR sensors from polarization properties measurement," Opt. Express **19**(2), 1656–1664 (2011), http://www.opticsinfobase.org/oe/abstract.cfm?URI=oe-19-2-1656.
23. C. Caucheteur, C. Chen, V. Voisin, P. Berini, and J. Albert, "A thin metal sheath lifts the EH to HE degeneracy in the cladding mode refractometric sensitivity of optical fiber sensors," Appl. Phys. Lett. **99**(4), 041118 (2011).
24. C. Caucheteur, V. Voisin, and J. Albert, "Polarized spectral combs probe optical fiber surface plasmons," Opt. Express **21**(3), 3055–3066 (2013), http://www.opticsinfobase.org/oe/abstract.cfm?URI=oe-21-3-3055.
25. V. Voisin, C. Caucheteur, P. Mégret, and J. Albert, "Interrogation technique for TFBG-SPR refractometers based on differential orthogonal light states," Appl. Opt. **50**(22), 4257–4261 (2011).
26. M. D. Baiad, M. Gagné, W.-J. Madore, E. De Montigny, N. Godbout, C. Boudoux, and R. Kashyap, "Surface plasmon resonance sensor interrogation with a double-clad fiber coupler and cladding modes excited by a tilted fiber Bragg grating," Opt. Lett. **38**(22), 4911–4914 (2013).
27. L. Novotny, "Strong coupling, energy splitting, and level crossings: a classical perspective," Am. J. Phys. **78**(11), 1199–1202 (2010).
28. A. Bialiayeu, C. Caucheteur, N. Ahamad, A. Ianoul, and J. Albert, "Self-optimized metal coatings for fiber plasmonics by electroless deposition," Opt. Express **19**(20), 18742–18753 (2011), http://www.opticsinfobase.org/oe/abstract.cfm?URI=oe-19-20-18742.

1. Introduction

Optical sensors based on the excitation of surface plasmon polaritons (SPPs) constitute an efficient tool to characterize and quantify molecular interactions and Surface Plasmon Resonance (SPR) sensing on gold surface remains the leading approach for label-free biosensing, due to its high resolution and robustness. In recent years, numerous SPR transducers have been developed around the seminal Kretschmann-Raether prism approach, which is exploited in most commercial systems [1]. In particular, optical fiber based sensors are particularly attractive for many reasons. Apart from their well-known qualities (lightweight, compact, remote operation in very small volumes, immunity to interference,...), fiber devices have two important advantages over other SPR configurations: light propagates essentially without loss in short lengths of fibers, resulting in very high signal-to-noise ratios, and interfacing devices to light sources and detectors consists essentially of plugging connectors into widely available fiber optic instrumentation, instead of having to carefully align optical beams through imaging systems. With continuous development and optimization, they will likely become perfectly suited for *in situ* diagnosis.

#230719 - $15.00 USD Received 16 Dec 2014; revised 15 Jan 2015; accepted 23 Jan 2015; published 30 Jan 2015

To excite surface plasmon resonance (SPR) in optical fiber plasmonic sensors, light confined in the fiber core is locally out-coupled and brought into contact with the surrounding medium. Practically, this is achieved either by polishing or etching the cladding so as to expose the evanescent wave to the surrounding medium or by using in-fiber gratings (refractive index modulations imprinted in the fiber core along the propagation axis). Hence, various architectures coexist: etched multimode optical fibers [2,3], side-polished optical fibers [4], D-type optical fibers [5,6], tapered optical fibers [7], U-shaped optical fibers [8], long period fiber gratings (LPFGs) [9] and tilted fiber Bragg gratings (TFBGs) [10]. Configurations based on cladding removal/decrease are the most straightforward to realize. The SPR is spectrally manifested by a broadband resonance (experimental full width at half maximum (FWHM) ~20 nm or higher) in the transmitted amplitude spectrum. Operation in reflection mode is possible by using a mirror after the sensing region. However, such configurations considerably weaken optical fibers at the sensor head and may prevent their use in practical applications, out of laboratory settings. For this reason, large core fibers (unclad 200-400 μm core) are used in practice [11,12]. These configurations operate at visible wavelengths, as usual for SPR sensing. However, the evanescent wave in the surrounding medium has a penetration depth that is proportional to the operation wavelength (λ). It usually ranges between λ/5 and λ/2, depending on the mode order [13]. Hence, operation at near-infrared telecommunication wavelengths enhances the penetration depth, which in turn improves the sensor sensitivity to large-scale targets such as proteins or cells. Operation in the near infrared can be easily achieved with gratings in single mode telecommunication fibers.

Gratings preserve the fiber integrity while providing a strong coupling between the core-guided light and the cladding. LPFGs consist in a periodic refractive index modulation of the fiber core with a period of a few hundreds of μm. They couple the forward-going core mode into forward-going cladding modes. Their transmitted amplitude spectrum is composed of a few wide resonances (FWHM ~20 nm) dispersed in a wavelength range of a few hundreds of nm. TFBGs are short period (~500 nm) gratings with a refractive index modulation slightly angled with respect to the perpendicular to the optical fiber axis. In addition to the self-backward coupling of the core mode, they couple light into backward-going cladding modes. Their transmitted amplitude spectrum displays several tens of narrow-band cladding mode resonances (FWHM ~100-200 pm) located on the short wavelength side of the Bragg resonance (or core mode resonance) corresponding to the core mode self-coupling. The core mode resonance provides an appropriate temperature and power reference, as it is not sensitive to SRI changes. According to phase matching conditions, every cladding mode resonance possesses its own effective refractive index and the maximum refractometric sensitivity is obtained when this effective index approaches the surrounding refractive index (SRI) value. Hence, TFBGs act as spectral combs and are the only optical fiber configuration able to probe simultaneously but distinctively all the optical fiber cladding modes.

SPR optical fiber sensors can be obtained from the above-listed structures when they are surrounded by a noble metal (most often gold or silver). Sheaths of thickness ranging between 30 and 70 nm are most generally used. It is worth mentioning that the optimum metal thickness for SPR coupling on optical fibers with 125 μm diameters is the same as for the planar equivalent (Kretschmann-Raether approach), for similar values of the glass and surrounding index. This is because the curvature of the cladding surface is two orders of magnitude smaller than the wavelength. SPR generation is achieved when the electric field of the light modes is polarized mostly radially at the surrounding medium interface (TM-like). Fiber modes with the orthogonal polarization state, i.e. azimuthal (or TE-like) are not able to excite the SPR, as their electric fields are tangent to the metal interface and thus cannot couple energy to the SPP. Depending on the configuration, sensitivities in the range [1e2 – 1e5 nm/RIU (refractive index unit)] have been reported for grating-assisted fiber SPR [14].

When comparing the sensor performances between different configurations, it is not sufficient to compare only sensitivities (i.e. wavelength shifts per refractive index change),

#230719 - $15.00 USD Received 16 Dec 2014; revised 15 Jan 2015; accepted 23 Jan 2015; published 30 Jan 2015

without considering the wavelength measurement accuracy. It is more appropriate to refer to the figure of merit (FOM) of the device. The FOM corresponds to the ratio between the sensitivity and the linewidth of the resonance, since it is easier to measure the exact location of a narrow resonance than a broad one [15]. In terms of experimentally demonstrated FOM, TFBGs surpass all configurations by more than one order of magnitude [14,16]. This results from both their sensitivity (~500 nm/RIU) and the narrowness of their resonances (< 200 pm).

Numerous publications have been devoted to the study and exploitation of plasmonic optical fiber sensors for enhanced refractometry and (bio)chemical sensing, through the use of bioreceptors (antibodies, aptamers, …) anchored on the metal surface. In this paper, using a complex mode solver and measurements on fabricated TFBGs, we numerically and experimentally analyze the intrinsic refractometric sensitivity of the optical fiber modes supported by a gold-coated telecommunication-grade single-mode optical fiber and we provide design rules for optimizing the FOM. The SPR mode is clearly identified in the spectral comb and the behavior of the small group of modes the spectral range of the SPR is tracked as a function of the SRI value. We clearly demonstrate that the refractometric sensitivity depends on the modal effective index (itself related to the SRI value) and that the global SPR envelope shift observed over an SRI change of 1e-2 or more can be ~25% bigger than the local SPR mode shift over a limited SRI change in a range of 1e-4. We also confirm that the optimum gold thickness for SPR generation lies in the range between 50 and 70 nm while a cladding diameter decrease from 125 μm to 80 μm enhances the refractometric sensitivity by ~20%. Finally, our study reveals that the ultimate refractometric sensitivity of cladding modes is ~550 nm/RIU when they are probed by near-infrared gold-coated TFBGs, and that this sensitivity is essentially the same as that of the equivalent prism configuration, apart from the fact that the fiber SPR linewidth can be more than 50 times narrower.

While TFBGs have already been used in biochemical applications [17–19], this study presents a full characterization of the vector cladding mode properties in gold-coated single-mode optical fibers in view of the optimization of the grating and metal layer properties towards achieving the ultimate FOM and hence the best limits of detection.

2. Numerical analysis

2.1 Finite-difference mode solver

The FIMMWAVE mode solver was used to compute the propagating modes in a standard single-mode optical fiber surrounded by a gold sheath. This software from Photon Design Inc. is a finite-difference complex mode solver in cylindrical coordinates. The following parameters were considered for the three-layered waveguide: 8.2 μm thick core with refractive index equal to 1.4504, 125 μm cladding with refractive index equal to 1.4440 surrounded by a gold sheath with a complex refractive index = 0.56-j11.4. Simulations yield the complex refractive index and the mode field of each propagating mode. The effective refractive index of a mode (further referred to $n_{eff,clad,i}$ with i = 1…N) corresponds to the real part of the complex refractive index while the mode loss is obtained from the imaginary part. For each mode computed by the solver, we use the TFBG phase matching conditions ($\lambda_{clad,i} = (n_{eff,core} + n_{eff,clad,i})\Lambda$ with i = 1…N) to estimate the corresponding resonance wavelength ($\lambda_{clad,i}$) [10]. This is obtained in the following by considering 1.4468 for the effective refractive index of the core mode ($n_{eff,core}$) and 557 nm for the grating period (Λ). Simulations were conducted to compute the TM_{0n} and EH_{1n} modes (radially-polarized modes) and the TE_{0n} and HE_{1n} modes (azimuthally-polarized modes).

The SPR mode can be identified either by finding the mode with the maximum loss or from mode field diagrams. Figure 1 shows the electric field patterns, decomposed into their radial and azimuthal components for three typical modes in the vicinity of the SPR. Mode $EH_{1,46}$ has the highest loss, a predominantly radial polarization, and a clear localization of the electric field at the metal-SRI boundary. The adjacent mode in the spectrum is a HE mode and

#230719 - $15.00 USD Received 16 Dec 2014; revised 15 Jan 2015; accepted 23 Jan 2015; published 30 Jan 2015

while it has almost exactly the same effective index (and is thus as well matched to the SPP as its EH neighbor) it does not couple efficiently to the SPP because its polarization is azimuthal. The other mode shown, $EH_{1,50}$, has the same polarization state as the $EH_{1,46}$ but its effective index is too far from the SPR for the grating to couple much energy to it. The behavior depicted in Fig. 1 is consistent across the whole mode spectrum and reflects an alternance between azimuthally- and radially-polarized modes. This alternation is present throughout the spectrum, except around the SPR where the presence of a SPP at the metal-SRI interface causes two radially-polarized modes to appear consecutively, as will be shown below.

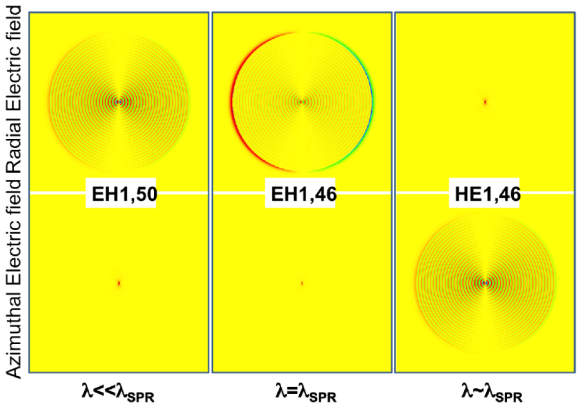

Fig. 1. Simulated electric fields pattern for three modes near the SPR, separated into radial (top row) and azimuthal (bottom row). All patterns have the same (normalized) mapping between magnitude and color. The three columns refer to cladding modes with effective indices of 1.3208, 1.3280, and 1.3285 (left to right).

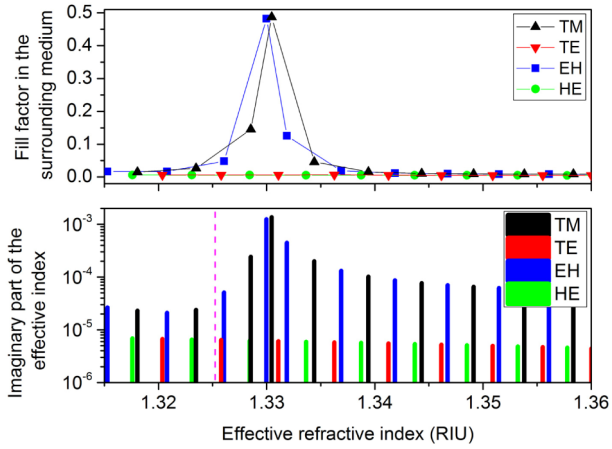

Fig. 2. Mode loss and fill factor in the surrounding medium as a function of the effective refractive index for a 50 nm gold-coated SMF immersed in water (the dashed line indicates the position of the 1D-SPP obtained with Eq. (1)).

The other way to identify the SPP mode consists in analyzing the complex refractive index of the modes. The mode with the highest loss (imaginary part of the mode effective index) has the highest fraction of mode power "propagating" in the metal and corresponds to the attenuation peak of the Kretschmann-Raether configuration. Figure 2 plots the imaginary part of the modal refractive index versus their real part for a 50 nm gold-coated SMF immersed in water (n = 1.315 at 1550 nm). To obtain a clear representation, the modes were sorted according to their azimuthal symmetry and dominant polarization. The SPR mode is obtained for a radial polarization and clearly appears as the one for which the attenuation is the highest, around 1.33. This picture also reveals the alternation between azimuthally- and radially-

#230719 - $15.00 USD Received 16 Dec 2014; revised 15 Jan 2015; accepted 23 Jan 2015; published 30 Jan 2015

polarized modes, except around the SPR where a TM mode follows an EH one. The percentage of the mode intensity in the surrounding medium – so-called fill factor – is also depicted in Fig. 2. It is the fill factor that contributes to increasing the refractometric sensitivity of optical fiber sensors to changes in the surrounding medium. While it stays around 1% and less for most of the modes, it suddenly increases for effective refractive indices close to 1.33, with a maximum reaching 50% for the SPR mode, confirming the large extraction of the mode field into the surrounding medium.

2.2 Influence of the gold layer thickness on the SPP sensitivity

Numerical simulations were conducted to identify the range of gold thicknesses suited to obtain a well-defined and sensitive SPR. We simulated different gold thicknesses (between 10 and 100 nm) in FIMMWAVE and analyzed the mode loss as a function of the effective refractive index, as depicted in Fig. 3.

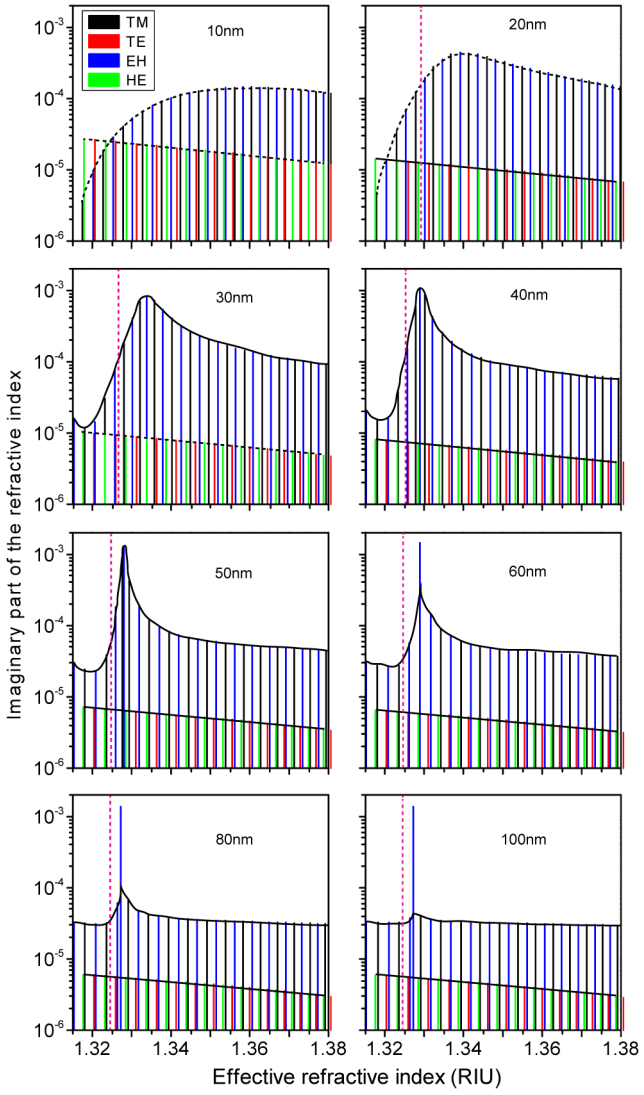

Fig. 3. Simulated mode loss for different thicknesses of the gold sheath. Each bar represents a mode with its effective index (abscissae) and loss (ordinate). Bars are color coded according to mode polarization and azimuthal order.

#230719 - $15.00 USD Received 16 Dec 2014; revised 15 Jan 2015; accepted 23 Jan 2015; published 30 Jan 2015

The envelope of the bar graphs (dashed line) of the TM and EH modes is an image of the envelope of the corresponding amplitude spectrum of the SPR-TFBG, as will be further illustrated in the following. Figure 3 clearly shows the emergence of the SPP mode for increasing gold thicknesses. At values lower than 30 nm, an SPP is excited but its envelope is very broad, yielding a poor resonance with limited refractometric sensitivity. Contrarily, for a gold thickness higher than 60 nm, the envelope becomes very narrow, consisting of a single lossy mode. While this would appear to be a desirable feature, it will be shown below that the most lossy mode is actually not useful as it disappears from the TFBG transmission spectrum (and so cannot be used in measurement), but most importantly that for those thicknesses the SPR mode becomes totally localized near the outer gold surface and becomes uncoupled from the fiber core, due to excessive attenuation across the gold film thickness. In short, when the film is too thick the SPR mode exists in theory (it then corresponds to a pure SPP of the outer gold surface) but it cannot be excited by light coming from inside the fiber. Hence, the analysis of the mode loss diagrams confirms that the correct thickness range for SPR generation is between 30 and 70 nm, which is the classical range of gold thickness used in most of optical fiber plasmonic biosensors, and indeed all kinds of plasmonic sensors [20]. Finally, for increasing gold thicknesses, the SPP mode is gradually blue-shifted, becoming closer to the cut-off refractive index.

As noted earlier, for the cladding diameter of normal un-modified optical fibers, the surface curvature is negligible relative to the light wavelength. Therefore, it is possible to design optimum metal layer thicknesses (further defined as the parameter *d*) using the well-known theoretical expressions for the planar one dimensional (1D) case [20]. The reflection of light incident from a high index medium (with relative permittivity $\epsilon_1 = 1.444^2$ silica glass) towards a lower index medium ($\epsilon_3 = 1.315^2$ for water) and through a metal layer with complex relative permittivity ϵ_2 (equal to −129.6-i12.8 for gold), as a function of wavelength and angle is given by Eq. (1) below. The material parameters are identical to those defined for the simulations in Section 2.1. For a given combination of media, a pronounced minimum occurs in the reflectance as a function of incidence angle or wavelength, as described in Eq. (1)-(3) [20]. This minimum corresponds to the excitation of a SPP at the metal-surrounding interface.

$$R = \left| \frac{r_{12}^p + r_{23}^p \exp\left(2ik_{z1}d\right)}{1 + r_{12}^p r_{23}^p \exp\left(2ik_{z1}d\right)} \right|^2 \tag{1}$$

With:

$$r_{mn}^p = \left(\frac{k_{zm}}{\epsilon_m} - \frac{k_{zn}}{\epsilon_n} \right) / \left(\frac{k_{zm}}{\epsilon_m} + \frac{k_{zn}}{\epsilon_n} \right) \tag{2}$$

Where the k_z are the wavevector magnitudes in the direction perpendicular to the interface (i.e. $\hat{z}$), with help from the parallel wavevector (continuous across the interfaces) associated with a given angle of incidence θ_i is k_x. The wavevectors are all defined in the following:

$$k_0 = \frac{2\pi}{\lambda} \tag{3a}$$

$$k_x = k_0 \sqrt{\epsilon_1} \sin(\theta_i) \tag{3b}$$

$$k_{z1} = \sqrt{k_0^2 \epsilon_1 - k_x^2} \tag{3c}$$

$$k_{z2} = \sqrt{k_0^2 \epsilon_2 - k_x^2} \tag{3d}$$

$$k_{z3} = \sqrt{k_0^2 \epsilon_3 - k_x^2} \tag{3e}$$

#230719 - $15.00 USD Received 16 Dec 2014; revised 15 Jan 2015; accepted 23 Jan 2015; published 30 Jan 2015

In order to compare the 1D SPP attenuation to the cladding mode spectrum, the angle of incidence is converted into an "effective index" for propagating in the x direction, through the grating phase matching equation given below:

$$n_{eff} = k_x / k_0 \tag{4}$$

The effective index of the planar SPP calculated using Eq. (1) and (4) is indicated by a dashed vertical line on Fig. 2 and 3. We will now investigate how the gold thickness modifies the bulk sensitivity of the fiber modes near the SPR.

Simulations were conducted to obtain the wavelength shift of the SPR and of the 1D-SPP caused by an SRI variation (6e-4 RIU by step of 2e-4 around the refractive index of water). The wavelength shift was computed from the effective refractive index by using the phase matching condition (Eq. (5)) for a TFBG with the parameters defined in Section 2.1. The results are given in Fig. 4 for gold thicknesses between 30 and 70 nm. As expected from the mode loss and from observations with unclad multimode fiber SPR sensors [21], the sensitivity increases with the gold thickness until saturation. In the case of gold-coated TFBGs, the sensitivity reaches its maximum around 550 nm/RIU. This value results from the fact that the SPR mode is observed in the amplitude spectrum of a TFBG at the following wavelength:

$$\lambda_{SPR} = (n_{eff,SPR} + n_{eff,core})\Lambda \tag{5}$$

Since neither $n_{eff,core}$ nor Λ are affected by the external medium, when the SRI changes by ∂n_{ext}, the wavelength of the SPR mode shifts by:

$$\frac{\partial \lambda_{SPR}}{\partial n_{ext}} = \frac{\partial n_{eff,SPR}}{\partial n_{ext}} \Lambda \tag{6}$$

As the effective index shift cannot be larger than that of the refractive index of any of its layers for an axially uniform waveguide, the maximum theoretical refractometric sensitivity is:

$$\frac{\partial \lambda_{SPR}}{\partial n_{ext}} \leq \Lambda \tag{7}$$

Equation (7) confirms that the SPR refractometric sensitivity is bound by the TFBG period. For comparison, the refractometric sensitivity for the SPP of a silica prism with 50 nm of gold in water at 1550 nm, calculated from the 1-D expression (Eq. (1) is 578 nm/RIU.

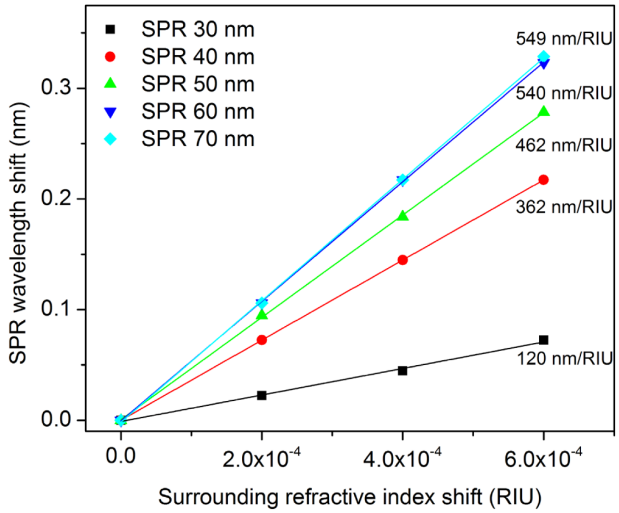

Fig. 4. Simulated refractometric wavelength shift of the SPR mode as a function of the gold sheath thickness.

#230719 - $15.00 USD Received 16 Dec 2014; revised 15 Jan 2015; accepted 23 Jan 2015; published 30 Jan 2015

Figure 5 depicts the SPP mode refractometric sensitivity in water as a function of the gold sheath thickness (red curve), extracted from the slopes of Fig. 4. It clearly shows an exponential trend, with a saturation beginning at a thickness of 60 nm. This sensitivity evolution is related to the fraction of optical power into the surrounding medium that is also depicted in Fig. 5 (blue curve). While the fraction of the SPR mode power in the surrounding medium continues to increase slightly between 70 and 100 nm, the fact that there is no longer any significant mode power near the core prevents the TFBG from coupling core guided light to this mode. The SPP at the metal outer surface becomes uncoupled from the cladding mode by an excessive thickness of gold.

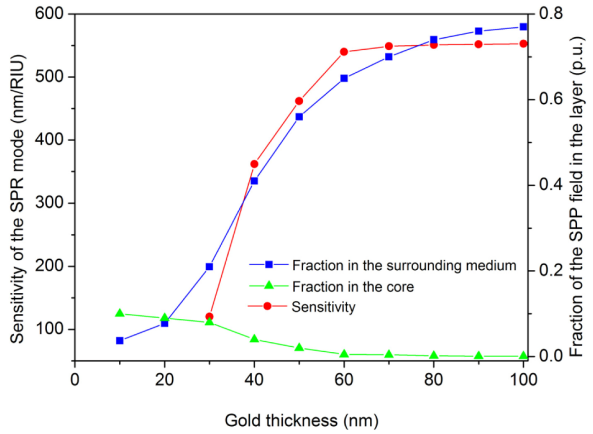

Fig. 5. Refractometric sensitivity of the SPP mode and fraction of its power in the surrounding medium as a function of the gold sheath thickness in the range 10-100 nm.

2.3 Influence of the optical fiber cladding thickness on the SPP sensitivity

In this section, an SMF coated with 50 nm of gold and immersed in water was considered and the cladding diameter was varied between 100 and 140 µm, as depicted in Fig. 6. Simulations confirm that the sensitivity of the SPR mode increases when the cladding diameter decreases. This behavior is quite obvious since the percentage of light into the surrounding medium increases when the cladding diameter decreases. Therefore, the SPR mode is more sensitive to refractive index variations. Interestingly, this figure also reveals that the optimum refractometric sensitivity is reached for a thickness around 100 µm.

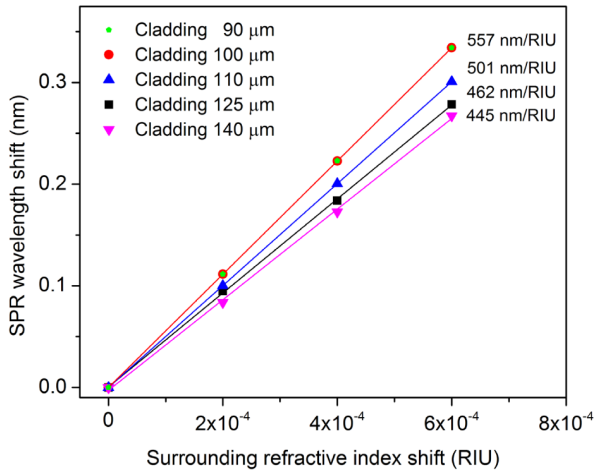

Fig. 6. Refractometric sensitivity of the SPR mode for different cladding diameters between 90 and 140 µm.

#230719 - $15.00 USD Received 16 Dec 2014; revised 15 Jan 2015; accepted 23 Jan 2015; published 30 Jan 2015

2.4 Influence of the surrounding refractive index value

In this section, we have used the FIMMWAVE mode solver to estimate the wavelength sensitivity of the SPR mode as a function of the starting value of the SRI. We computed the effective refractive index of the SPR mode for a sensor with a 50 nm gold coating and considering a long range of SRI values (between 1.315 and 1.425 by steps of 2e-4 RIU). Figure 7 depicts the evolution of the SPR wavelength as a function of the SRI value. It can be seen that the evolution is globally linear with sensitivity equal to 572 nm/RIU (based on a linear fit of the raw data). Upon closer examination, the insets of the figure highlight the hopping of the SPR from one cladding mode to another, detected by a discontinuity in the evolution. Apparently, the SPP becomes phase matched to a sequence of different cladding modes one after another (according to the SRI value), and when such phase matching occurs the SPP "drags" the corresponding cladding mode index at a much higher rate. Depending on which cladding mode is matched to the SPP, the SPR does not exhibit the same sensitivity. For instance, the SPR mode presents a sensitivity of 464 nm/RIU for an SRI around 1.324 and 408 nm/RIU around 1.401.

Figure 7 also confirms that, similarly to what is already reported experimentally in [22–26], the global SPR shift computed over a wide SRI range exceeds the local SPR shift, the latter being bounded by the TFBG periodicity, as mentioned above. This discrepancy is linked to the evolution of the SPR envelope that does not account for mode hopping.

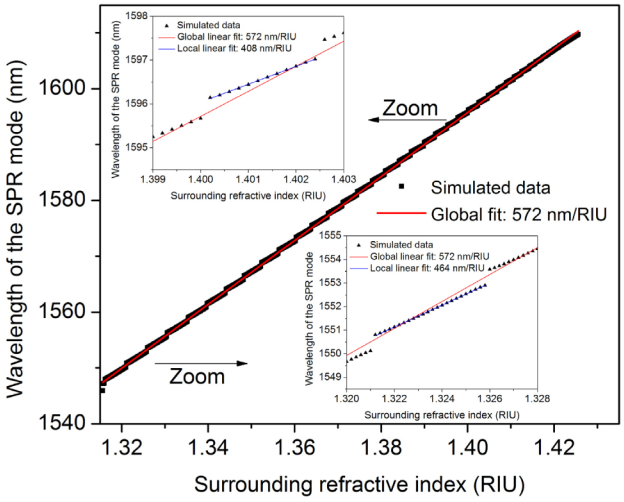

Fig. 7. Wavelength shift of the SPR mode as a function of the SRI for a 50 nm gold-coated SMF.

Figure 8 depicts the refractometric sensitivity of the SPR mode as a function of the SRI in the range 1.32-1.42. Hence, the ordinates of Fig. 8 correspond to the sensitivities computed from a linear regression of the modal wavelength evolutions in their corresponding range of sensitivity. Abscissas are the middle of the linear range covered by their corresponding mode. The evolution exhibits a nonlinear trend with a minimum (406 nm/RIU) around 1.405 and a maximum (495 nm/RIU) above 1.420. The range of the change in sensitivities is of the order of ~18%. In water, the sensitivity is close to its maximum value, which is beneficial for high resolution (bio)chemical sensing.

2.5. Bulk sensitivity of other modes

Carrying out the same characterization for cladding modes near the SPR one, a smaller sensitivity is obtained, which was already highlighted in [24]. This behavior is depicted in Fig. 9 for a 50 nm gold-coated SMF. The modes located to the left(right) of the SPR one are

#230719 - $15.00 USD Received 16 Dec 2014; revised 15 Jan 2015; accepted 23 Jan 2015; published 30 Jan 2015

labeled SPR + i(SPR-i) with i increasing when going further from the SPP location. It is shown that sensitivity rapidly drops to less than 50 nm/RIU for modes away from the SPR. This results from the poorer extraction of the modes into the external medium, as depicted in Fig. 2.

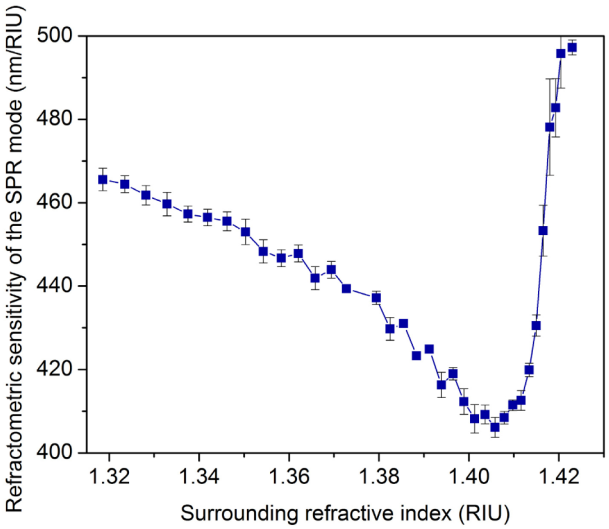

Fig. 8. Wavelength sensitivity of the SPR mode as a function of the SRI for a 50 nm gold-coated SMF.

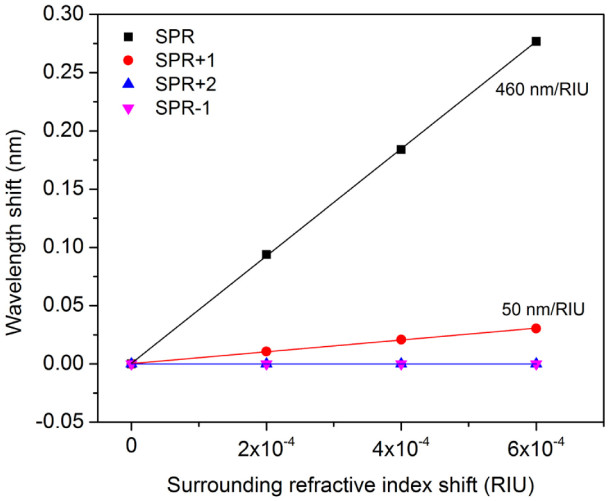

Fig. 9. Wavelength shift of different modes as a function of the SRI for a 50 nm gold-coated SMF.

2.6. SPP hopping as a function of the surrounding refractive index value

To conclude this section dedicated to the numerical analysis, we would like to report on an observation that was made when analyzing the data. The bar charts of Fig. 2 and 3 clearly depict a continuous alternation between radially- and azimuthally-polarized modes. As previously mentioned, this alternation is broken at the SPR location where two radially-polarized modes appear consecutively. Furthermore, the inset of Fig. 7 shows that the "SPR" mode (i.e. the cladding mode which becomes sensitive to the SRI when phase matched to the SPP) shifts discontinuously between adjacent cladding modes when the SRI changes by

#230719 - $15.00 USD Received 16 Dec 2014; revised 15 Jan 2015; accepted 23 Jan 2015; published 30 Jan 2015

sufficiently large amounts. To bring an additional insight into this particular behavior, the refractometric wavelength shift of a sub-group of radial modes in the vicinity of the SPR (labeled arbitrarily from EH-1 to EH-4) is shown in detail in Fig. 10. It becomes clear that when a mode effective index approaches the effective index of a SPP, its sensitivity increases from ~20 nm/RIU to nearly 500 nm/RIU, for a SRI range of ~5e-3. At the end of this range, the SPP phase matching condition jumps to the next radial mode with the consequence that the high sensitivity slope is transferred to the new cladding mode. This switching of modes as a function of the surrounding refractive index value presents similarities with the phenomenon of mode anticrossings, as reported in [27] for the resonances of weakly coupled oscillators. In our case the two "oscillators" are the resonant coupling between the core mode and a cladding mode, and the other resonant coupling between the cladding mode and the SPP. We will not go further into such considerations here but we hope that this observation can foster further studies in the analogies between grating-assisted SPR structures and coupled oscillators.

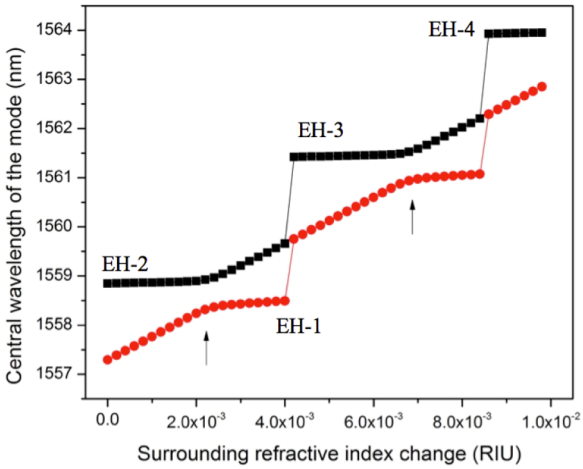

Fig. 10. Wavelength shift of the SPR mode and its radially-polarized neighbor as a function of the SRI value.

3. Experimental validation

Experiments were carried out with 1cm-long TFBGs manufactured into hydrogen-loaded telecommunication grade single-mode optical fiber using a 1090 nm period uniform phase mask and a frequency-doubled Argon-ion laser emitting at 244 nm. Tilting has been obtained by rotating the phase mask around the axis of the writing beam. An external tilt angle between 6° and 10° was chosen with respect to the plane perpendicular to the optical fiber axis to ensure a strong coupling to cladding modes having an effective refractive index close to water (1.315 at 1550 nm). Right after the inscription process, the gratings were annealed at 100 °C for 24 hours to remove the residual hydrogen and to stabilize their physical properties. A gold sheath was then deposited on the TFBGs using a sputtering process, as described in [23].

Figure 11 depicts the insertion loss spectrum of a 1 cm long 8° TFBG coated by a 30 nm thick gold layer and immersed in salted water. Orthogonally-polarized spectra (corresponding to the radial and azimuthal polarizations) were measured with an optical vector analyzer from Luna Technologies. A linear polarizer placed between the optical source and the TFBG was used to control and optimize the input state of polarization. As explained in [22–26], the radial polarization spectrum presents a strong extinction of the resonances around 1542.5 nm, corresponding to the transfer of energy to the SPP while the azimuthal polarization spectrum remains almost unaffected by the lossy gold layer. Figure 11 also displays the results of a simulation conducted with similar parameters as in the experiments. A nearly perfect agreement is obtained in the wavelength positioning between the experiments and the

#230719 - $15.00 USD Received 16 Dec 2014; revised 15 Jan 2015; accepted 23 Jan 2015; published 30 Jan 2015

simulation, confirming the validity of our theoretical analysis. Let us note that Fimmwave cannot easily compute modes with effective indices lower than the SRI, i.e. modes below the cladding mode cut-off which is located here around 1534 nm.

The effect of the gold coating thickness on the TFBG spectral content was also investigated. For this, different gold thicknesses were deposited using the sputtering chamber, in which a Quartz microbalance thickness monitor was used to estimate the thickness of the gold layer on the fiber. Figure 12 depicts the results for radially polarized spectra measured in salted water. As predicted in Fig. 3, increasing gold thickness up to ~50 nm lead to a blue shift of the SPR mode (while the cut-off location remains unaffected), as well as a narrowing and deepening of the envelope of lossy modes (those with decreased resonance amplitude). For gold thicknesses thicker than 70 nm, the radially polarized spectrum retrieves its shape as if there was no gold, essentially due to the strong attenuation of light in the gold coating and the impossibility to couple to the SPP across such thick metal coating [28].

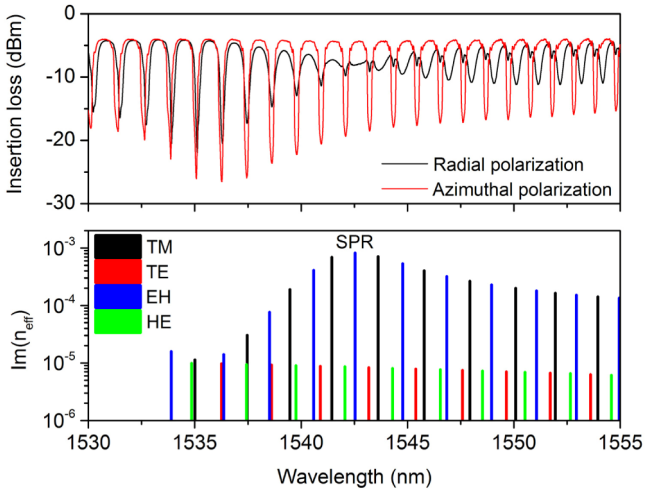

Fig. 11. Radial and azimuthal polarization modes spectra of a 30 nm gold-coated 8° TFBG immersed in water (top) and corresponding Fimmwave simulation (bottom).

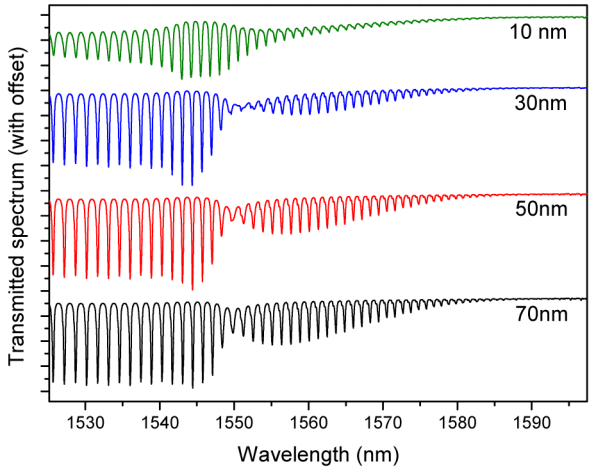

Fig. 12. Transmitted spectrum (radial polarization) of an 8° TFBG immersed in salted water for different gold coating thicknesses.

#230719 - $15.00 USD Received 16 Dec 2014; revised 15 Jan 2015; accepted 23 Jan 2015; published 30 Jan 2015

Finally, gold-coated TFBGs were immersed in different refractive index liquids to measure their refractometric sensitivity (this experimental demonstration is similar to the one published in [16], but repeated here for completeness). Figure 13(a) shows the transmitted amplitude spectra of a 50 nm gold-coated TFBG measured for 3 different refractive index values. For such large SRI changes, the SPR location can be unambiguously located by following the strongest attenuation in each spectrum. Therefore, the interrogation relies on the tracking of the wavelength shift of the center of the envelope of the most attenuated resonances. Using this technique, the SRI sensitivity is ~550 nm/RIU in the range between 1.32 and 1.42 (Fig. 13(b)), in good agreement with the numerical predictions.

For high-resolution refractometric sensing over an SRI range limited to 1e-3 typically, accurate measurements of the SPR mode are not possible from the radially polarized spectrum taken alone. Indeed, the SPP is only revealed by its absence from the spectrum and it cannot be reliably measured for wavelength shifts limited to a few picometers. Hence, different methods have been developed to track the SPR shift, mainly based on a comparison between both orthogonally-polarized amplitude spectra as reported in several prior experimental papers related to this one [22,24,25], and they will not be detailed here. In practice, modes slightly off the SPR are used, because they combine relatively high sensitivity with a narrow spectral width and they can be "followed" by a combination of their changes in amplitude and wavelength. Indeed, as they stand on the shoulder of the SPR envelope, a slight change of the SPP location yields a modification of the peak-to-peak amplitude of these modes, as exploited in [17–19].

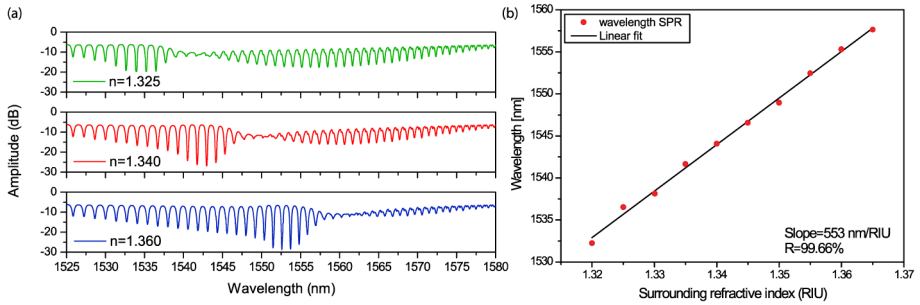

Fig. 13. SPR signature in the transmitted spectrum of gold-coated TFBG for coarse changes in SRI (a) and SPR tracking for different SRI values (b).

Such high resolution sensing is demonstrated in Fig. 14 with spectra measured during a biochemical binding experiment, i.e. for a SPR shift close to the detection limit (a full report on these experiments can be found in [17]). By zooming in on resonances near the SPR and a few nm away, it becomes clear that the presence of a comb of resonances with widely different sensitivities allows for very small wavelength shifts to be detected unambiguously with high precision.

#230719 - $15.00 USD Received 16 Dec 2014; revised 15 Jan 2015; accepted 23 Jan 2015; published 30 Jan 2015

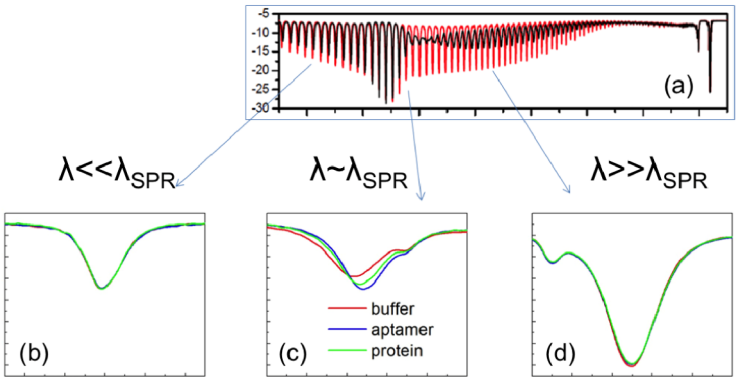

Fig. 14. Spectra measured during a biosensing experiment (a) with 3 spectral regions shown in detail: on the short wavelength side of the SPR (b); near the SPR (c); and on the long wavelength side (d).

4. Conclusion

In this work, we have numerically and experimentally analyzed the intrinsic refractometric sensitivity of optical fiber modes supported by a gold-coated telecommunication-grade single-mode optical fiber at near infrared wavelengths. We have shown that the SPR mode can be clearly identified in the spectral comb and that its refractometric sensitivity is dependent on various external parameters (gold thickness, cladding thickness and surrounding refractive index value). In particular, we have shown that the refractometric sensitivity is not monotonic as a function of the surrounding refractive index. It depends on the cladding mode order and shows discontinuities when switching from one cladding mode to another. The sensitivity reaches its maximum value for aqueous solutions with a refractive index close to water, with an ultimate value close to 570 nm/RIU. Comparisons with the Kretschmann-Raether configuration with the same materials (silica prism, gold film, and water-like surroundings) further showed that the TFBG can achieve similar sensitivities (within 5%), with the important side benefit of a significantly narrower resonance linewidth (0.1 nm vs at least 5 nm).

While TFBGs have already been successfully used in biochemical applications, this study brings a full understanding of the modal behavior in gold-coated single-mode optical fibers and is therefore particularly useful for design purposes. We hope that it will foster future research works involving plasmonic effects and cladding mode resonances.

Acknowledgment

Christophe Caucheteur is supported by the Fonds National de la Recherche Scientifique (F.R.S.-FNRS). This research has been conducted in the frame of the ERC (European Research Council) *Starting Independent Researcher Grant* PROSPER (grant agreement N° 280161 – http://www.umons.ac.be/erc-prosper). Jacques Albert holds the *Canada Research Chair in Advanced Photonic Components* at *Carleton University* and this research is funded by NSERC.

#230719 - $15.00 USD Received 16 Dec 2014; revised 15 Jan 2015; accepted 23 Jan 2015; published 30 Jan 2015